Poly(ε-caprolactone)-Functionalized Carbon Nanofibers by Surface-Initiated Ring-Opening Polymerization

Kai Wang, Wenwen Li, Chao Gao

College of Chemistry and Chemical Engineering, Shanghai Jiao Tong University, Shanghai 200240, People's Republic of China

Received 24 September 2006; accepted 24 January 2007
DOI 10.1002/app.26285
Published online 28 March 2007 in Wiley InterScience (www.interscience.wiley.com).

ABSTRACT: Carbon nanofibers (CNFs) were covalently functionalized with biodegradable poly(ε-caprolactone) (PCL) by *in situ* ring-opening polymerization (ROP) of ε-caprolactone in the presence of stannous octoate. Surface oxidation treatment of the pristine CNFs afforded carboxylic CNFs (CNF-COOH). Reaction of CNF-COOH with excess thionyl chloride ($SOCl_2$) and glycol produced hydroxyl-functionalized CNFs (CNF-OH). Using CNF-OH as macroinitiator, PCL was covalently grafted from the surfaces of CNFs by ROP, in either the presence or absence of sacrificial initiator, butanol. The grafted PCL content was achieved as high as 64.2 wt %, and can be controlled to some extent by adjusting the feed ratio of monomer to CNF-OH. The resulting products were characterized by FTIR, NMR, Raman spectroscopy, TGA, DSC, SEM, TEM, HRTEM, and XRD. Core–shell nanostructures were observed under HRTEM for the PCL-functionalized CNFs because of the thorough grafting. The PCL-grafted CNFs showed different melting and crystallization behaviors from the mechanical mixture of PCL and CNF-OH. This approach to PCL-functionalized CNFs opens an avenue for the synthesis, modification, and application of CNF-based nanomaterials and biomaterials. J Appl Polym Sci 105: 629–640, 2007

Key words: carbon nanofibers; composites; biocompatibility; TEM; differential scanning calorimetry

INTRODUCTION

Carbon nanomaterials are a particularly fascinating subclass of nanomaterials, since different conformation or morphology of nanocarbons may show extremely different or even opposite properties from each other. Carbon nanomaterials mainly include fullerenes,[1] carbon nanotubes (CNTs),[2,3] carbon nanofibers (CNFs),[4] carbon nanocones[5] or horns,[6] carbon spheres,[7] and nanodiamonds.[8] Functionalization of carbon nanomaterials is a powerful strategy to improve their solubility or wettability, realize their potential in a wide range of application, and prepare novel materials with tailor-made structures and properties.[9,10] In this regard, functionalization of carbon nanomaterials with polymers or biomacromolecules is of particular interest, because different properties of both materials can be integrated into one hybrid object.[11] For instance, different types of polymeric fullerene derivatives, including main-chain, side-chain, star-shaped, and fullerene-end-capped ones, have been prepared successfully.[12] Grafting polymer from surfaces of carbon black[13] or carbon spheres[14] by surface-initiated atom transfer radical polymerization (ATRP) has been realized. Polymeric functionalization of quantum-sized carbon dots for bright and colorful photoluminescence[15] and immobilization of DNA onto the carbon nanodots[16] have also been reported. Significantly, polymer-functionalized CNTs have also been widely addressed because of the unique properties and tremendous potential of CNTs. Up to now, polymers made from (meth)acrylic,[17–19] styrenic[20] and acrylamide-type monomers,[21] and polyolefin,[22] polyether,[23] polyester,[24] polyamide,[25] polyimide,[26] polyurea,[27] polyurethane,[28] and polyaniline,[29] etc., have been successfully grafted from/to surfaces of CNTs by means of controlled/living radical polymerization, radical polymerization, anionic or cationic polymerization, polycondensation, esterification, radical coupling, and so forth via the so-called *grafting from* or *grafting to* strategy. The grafting to method means direct attachment of polymers with functional or reactive groups to a substrate.[30] The grafted content is often limited due to the steric hindrance effect and low reactivity of macromolecules.[31] By contrast, in the grafting from strategy, polymer brushes are grown

Correspondence to: C. Gao (chaogao@sjtu.edu.cn).
Contract grant sponsor: National Natural Science Foundation of China; contract grant numbers: 50473010, 20304007.
Contract grant sponsor: Foundation for the Author of National Excellent Doctoral Dissertation of China; contract grant number: 200527.
Contract grant sponsor: Fok Ying Tung Education Foundation; contract grant number: 91013.
Contract grant sponsor: Opening Research Foundation, Key Laboratory of Molecular Engineering of Polymers, Ministry of Education, Fudan University.

from a substrate by surface-initiated *in situ* polymerization of monomers.[17–19,21] This strategy makes controlled/living polymerization on a substrate accessible, resulting in good controllability on the content and structure of the grafted polymer.[17–19,21]

Functionalization of CNFs with polymers is also of intriguing interest to both scientists and engineers. CNFs are considered as analogs of CNTs, and have comparatively excellent properties of CNTs such as high electric and thermal conductivity and strong mechanical strength. Therefore, CNFs can replace CNTs in some applications such as polymer additives,[32] gas storage materials,[33] electrode for fuel cell,[34] and catalyst supports.[35] Accordingly functionalizing CNFs with polymers and investigating corresponding polymerization principles in the presence of CNFs are of significance. Lukehart and coworkers prepared hydrophobic and hydrophilic polymer brushes on surfaces of graphitic CNFs using ATRP.[36] Tan and coworkers functionalized vapor-grown CNFs with *meta*-poly(ether-ketone) via *in situ* polycondensation of 3-phenoxybenzoic acid in poly(phosphoric acid).[37] Hamers and coworkers covalently modified CNFs with DNA.[38] Polyaniline-coated CNFs were also fabricated by a technique of one-step vapor deposition polymerization.[39] By the way, small organic molecule-functionalized CNFs were also reported recently.[40]

Considering potential applications of functionalized CNFs in bionanotechnology, herein, we graft biodegradable poly(ε-caprolactone) (PCL)[24,41] from surfaces of CNFs by *in situ* ring-opening polymerization (ROP). The resulting PCL-grafted CNFs can be relatively well dispersed in common organic solvents, such as tetrahydrofuran (THF) and chloroform. The covalent grafting between PCL and CNFs was confirmed by the measurements of hydrogen nuclear magnetic resonance (NMR), Fourier-transform infrared (FTIR), transmission electron microscopy (TEM), scanning electron microscopy (SEM), differential scanning calorimetry (DSC), and XRD.

EXPERIMENTAL

Materials

Vapor-grown CNFs were donated from Showa Denko of Japan (150 nm in diameter and 10–20 μm in length). The monomer, ε-caprolactone (Acros, 99%), was dried over CaH_2 at room temperature for 48 h and distilled under reduced pressure. Butyl alcohol and ethylene glycol were purchased from Zhengxin Chemical (Shanghai, China), distilled under reduced pressure, and stored in the presence of 4-Å molecular sieves. Stannous octoate was purchased from Sigma-Aldrich and used as received. THF, methanol, and other organic reagents or solvents were obtained from Shanghai Reagent and used as received.

Instrumentation

FTIR spectra were recorded on a PE Paragon 1000 spectrometer. ^{1}H NMR spectra were measured with a Varian Mercury Plus 400 MHz spectrometer, using $CDCl_3$ as the solvent. Molecular weights were measured by gel permeation chromatography (GPC) using PE series 200, with PS as standards and THF as the eluent at a flow rate of 1 mL/min. Thermal gravimetric analysis (TGA) was conducted on a PE TGA-7 instrument with a heating rate of 20°C/min in a nitrogen flow (20 mL/min). Raman spectra were recorded on a LabRam-1B Raman spectroscope operating at a laser wavelength of 632 nm. SEM images were recorded using a LEO 1550VP field-emission microscope. TEM analysis was performed on JEOL JEM2010 and high-resolution TEM (HRTEM) was conducted on JEOL JEM 2100F, and they were operated at 200 kV. Photographs of the samples in solvents were taken using a digital camera (Sony, DSC-S70). DSC was performed under a nitrogen atmosphere, with heating and cooling rates of 10°C/min using a Perkin-Elmer Pyris-1. Wide-angle X-ray diffraction (WAXD) of compressed-molded specimens was recorded on a Rigaku X-ray diffractometer D/MAX-2200/PC, with Cu Kα radiation (40 kV, 20 mA) at a rate of 4.0°/min over the range of $5^\circ < 2\theta < 40^\circ$.

Acid treatment of CNFs

In a typical experiment, 5 g of crude CNFs were added into a 250 mL round-bottom flask, with 100 mL mixture of concentrated sulfuric acid (98%) and nitric acid (60%) (3:1 by volume). The mixture was sonicated in a bath (40 Hz) for 10 min and then heated to reflux (120°C) for 2 h. After cooling to room temperature, the mixture was diluted with 800 mL of deionized water and then filtered with 0.22-μm Milipore polycarbonate membrane. The black solid was then redispersed in water and filtered again. The dispersing and filtration steps were repeated at least four cycles, until the pH of the filtrate approached 7. The final black solid was collected by centrifuging and then dried under vacuum for 24 h at 60°C, giving rise to 3.5 g (~ 70% of yield) of carboxylic CNFs (CNF-COOH).

Synthesis of CNF-OH

Typically, the as-prepared CNF-COOH (2 g) was dispersed in $SOCl_2$ (80 mL) and stirred at 70°C for 24 h. The residual $SOCl_2$ was removed by reduced pressure, giving acyl chloride-functionalized CNFs (CNF-COCl). Glycol (80 mL) was mixed with CNF-COCl and the mixture was stirred at 120°C for 48 h. The solid was collected after repeated washing and filtration with THF, using the Milipore membrane as mentioned earlier. After drying under vacuum over night

TABLE I
Reaction Conditions and Selected Results for Grafting Poly(ε-caprolactone) from the Surfaces of Carbon Nanofibers (CNFs)

Sample	R_{wt}[a]	R_{mol}[b]	f_{wt}[c] (%)	Conv[d] (%)	$M_{n,theo}$[e]	$M_{n,conv}$[f]	M_n[g]	PDI[g]
PCL	13.48/0.12/–	73/1/–	–	61	8327	5079	4230	1.19
CNF-PCL1	3.37/0.12/0.1	417/22.8/1	19.8	90	2086	1877	1870	5.86
CNF-PCL2	6.76/0.12/0.1	837/22.8/1	21.9	81	4187	3391	3130	4.71
CNF-PCL3	13.48/0.12/0.1	1669/22.8/1	29.5	55	8350	4592	3480	4.48
CNF-PCL4	26.96/0.12/0.1	3338/22.8/1	32.7	42	16700	7014	6340	1.99
CNF-PCL5	3.37/–/0.1	417/–/1	39.7	10	–	–	5200	4.58
CNF-PCL6	13.48/–/0.1	1669/–/1	64.2	5	–	–	8270	1.49

[a] The weight feed ratio of ε-caprolactone/butyl alcohol/CNF-OH; for PCL, R_{wt} is the weight feed ratio of ε-caprolactone/butyl alcohol, and for CNF-PCL5 or CNF-PCL6, R_{wt} is the weight feed ratio of ε-caprolactone/CNF-OH.
[b] The mole feed ratio of ε-caprolactone/butyl alcohol/CNF-OH.
[c] The grafted PCL weight fraction calculated from TGA data.
[d] The conversion of ε-caprolactone. For samples of CNF-PCL1-4, it is calculated from the weight ratio of the free PCL to monomer; for samples of CNF-PCL5 (free PCL is 0.27 g) and CNF-PCL6 (free PCL is 0.5 g), it was calculated from the weight ratio of (free PCL + grafted PCL)/monomer.
[e] Theoretical molecular weight, $M_{n,theo} = R_{mol} \times$ ε-caprolactone molar mass (114.14).
[f] $M_{n,conv} = M_{n,theo} \times$ conversion.
[g] The number-average molecular weight (M_n) and polydispersity index (PDI) of the free polymer measured by GPC.

at 60°C, 1.8 g of hydroxyl functionalized CNFs (CNF-OH) was obtained.

Synthesis of PCL-grafted CNFs

Typically (CNF-PCL3 in Table I), the as-prepared CNF-OH (0.1 g) was added into a 25 mL round-bottom flask, which was then dried under vacuum at 80°C for 2 h to remove any traces of water. The flask was sealed with a rubber plug. Butyl alcohol (0.12 g, 1.6 mmol) and ε-caprolactone (13.48 g, 0.118 mol) were injected into the flask using degassed syringes, respectively. The flask was evacuated and filled thrice with high-purity nitrogen to eliminate the influence of oxygen. Then, 4.05 mg (0.03 wt % of the ε-caprolactone) of stannous octoate was injected, and the mixture was stirred at 120°C in an oil bath for 24 h. The viscosity of the mixture was increased gradually, indicating that polymerization occurred. After 24 h, the mixture was too viscous to stir. After cooling to room temperature, the mixture was dissolved in 300 mL THF, sonicated in a bath (40 Hz) for several minutes, and filtered subsequently. The free PCL was obtained from the filtrate by precipitation into methanol. The black solid was then redispersed in THF and filtered again. The dispersing and filtration steps were repeated at least four cycles to remove the ungrafted polymer in the product (no precipitation was observed when the filtrate was added to methanol). The final solid product of PCL-grafted CNFs (CNF-*g*-PCL) was then collected by centrifuging from the THF solution.

The same protocol was employed to prepare the CNF-PCL5 and CNF-PCL6 (Table I), except that no butyl alcohol was added as a sacrificial initiator.

Also, control experiments of butanol-initiated polymerization of ε-caprolactone in the presence of CNF-COOH or pristine CNFs were conducted. The synthesis steps and feed ratios were the same as the case of CNF-PCL3 (Table I), except that CNF-OH was replaced by CNF-COOH or pristine CNFs.

RESULTS AND DISCUSSION

Owing to the biodegradation and biocompatibility, PCL is widely used in scientific research as well as in industries such as biomedicine and environmental friendly wrapper. PCL-functionalized surfaces or substrates, such as silica (~ 30 nm) or cadmium sulfide (~ 1.5 nm) nanoparticles,[42] γ-Fe_2O_3 nanoparticles,[43] and starch-like polysaccharides,[44] etc., have been achieved.[45] However, as far as we know, PCL-grafted CNFs were not reported yet. To functionalize CNFs with PCL and to integrate the unique properties of both materials into one hybrid nanomaterial, beyond all doubt, is of great interest and significance. Herein, we focus on the synthesis and characterization of PCL-functionalized CNFs. The mechanical, electrical, and other properties and applications of the resulting hybrid nanomaterials will be addressed later.

Preparation of CNF-OH macroinitiator

To graft PCL from the surfaces of CNFs by ROP via the grafting from approach, hydroxyl-functionalized CNFs (CNF-OH) were first synthesized as macroinitiators. Figure 1 shows the synthesis steps. It was reported that oxidative acid treatment is one of the effective methods to introduce functional groups such as carboxyl ones on CNFs[36] or CNTs.[18] Herein, the mixture of concentrated H_2SO_4 and HNO_3 (1 : 3 by

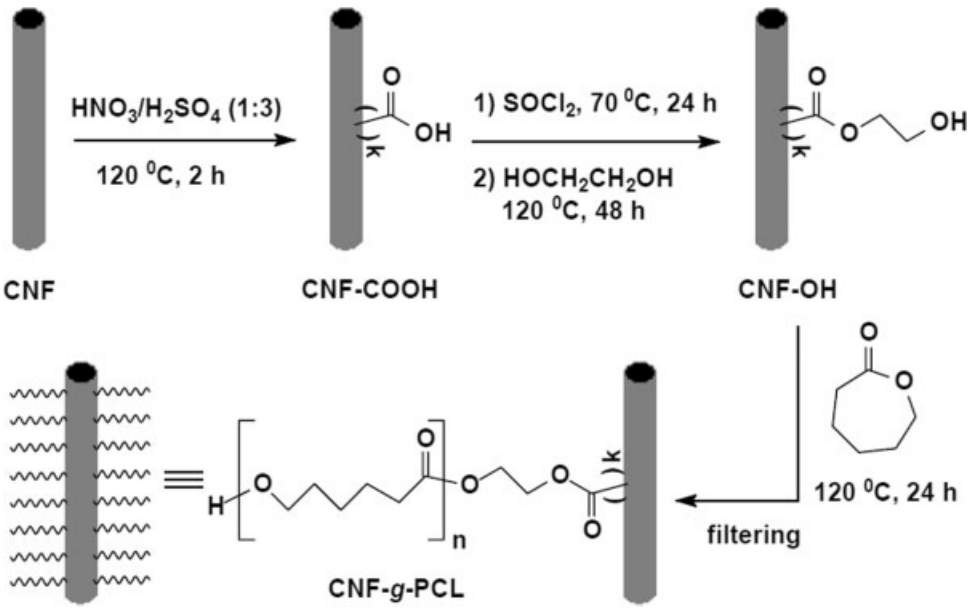

Figure 1 Synthesis of PCL-grafted CNFs.

volume) was used to oxidize CNFs, affording carboxylic CNFs (CNF-COOH). CNF-COOH was then reacted with excess $SOCl_2$, resulting in acyl chloride-functionalized CNFs (CNF-COCl). The CNF-COCl was subsequently reacted with excess glycol, producing the macroinitiator of CNF-OH. TGA, shown in Figure 2, indicates that the weight-loss of the pristine CNFs is 1.0% from 240°C to 440°C and 3.2% at 800°C, respectively. The weight loss of CNF-OH is 6.3% from 240°C to 440°C. Hence, the hydroxyl content covalently anchored on CNFs is about 5.3 wt %, corresponding to ~ 0.60 mmol/g of hydroxyl density of CNF-OH. From the surface area of CNFs (~ 65 m^2/g), we calculated the average surface density of hydroxyl to be ~ 56 hydroxyl/10 nm^2. As a comparison, for hydroxyl-functionalized multiwalled carbon nanotubes (MWNT-OH) prepared with the similar process, the hydroxyl density can reach ~ 1.06 mmol/g (~ 54 hydroxyl/10 nm^2 assuming the surface area of the MWNTs is 120 m^2/g).[24] This can be explained by the fact that the surface area of CNFs is much lower than that of MWNTs with the same mass, because of the larger diameter.

PCL was grown from the surfaces of CNFs, with CNF-OH as the macroinitiator by ROP of ε-caprolactone in bulk, in the presence of stannous octoate (Fig. 1). Different contents of PCL were covalently grafted from the surface of CNFs by controlling the feed ratio of monomer to the initiator. The reaction conditions and selected results are listed in Table I.

Two initiating manners were tried comparatively with sole CNF-OH and a mixture of CNF-OH and butyl alcohol as initiator. In the presence of the sacrificial initiator of butyl alcohol, both CNF-OH and butyl alcohol can initiate the ROP of ε-caprolactone, resulting in PCL-grafted CNFs and free PCL. The free PCL can be collected and used to estimate the molecular weight of the grafted polymer. Four experiments with different ratios of monomer to the coinitiator, but the same ratio of butyl alcohol to CNF-OH, were performed. When the feed ratio of monomer/butyl alcohol/CNF-OH was increased from 417/22.8/1 to 3338/22.8/1, the conversion of ε-caprolactone monomer decreased from 90% to 42%, most likely due to the higher viscosity in the case of greater feed ratio when the polymerization approaches a certain degree. The theoretical molecular weight we have designed through the feed ratio of monomer to initiators is from 2086 to 16,700 g/

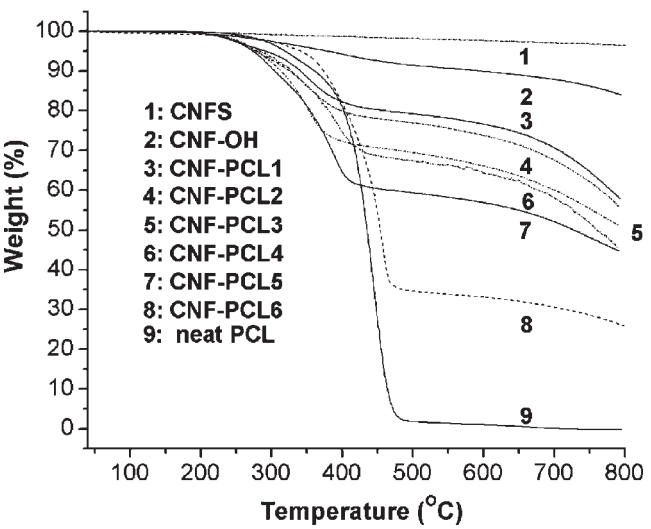

Figure 2 TGA curves of pristine CNFs, CNF-OH, CNF-*g*-PCL, and neat PCL.

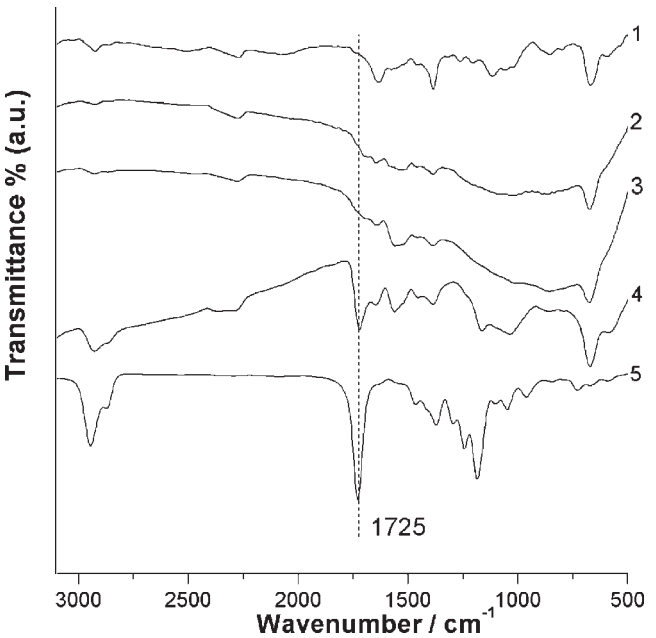

Figure 3 FTIR spectra of (1) pristine CNFs, (2) CNF-COOH, (3) CNF-OH, (4) CNF-PCL5, and (5) neat PCL.

mol at a full conversion. Although the conversion of monomer decreased with increase in the feed ratio, the number-average molecular weight (M_n) of the free PCL calculated from the monomer conversion still increased (Table I). GPC data confirmed our supposition, the M_n of the free PCL increased from 1870 to 6340 g/mol. Correspondingly, the weight fraction of PCL grafted on CNFs ($f_{wt\ \%}$) increased regularly from 19.8 to 32.7 wt % (Fig. 2 and Table I), which can be possibly attributed to the increase of M_n of PCL grafted on the CNFs. This indicates that the grafted polymer amount on CNFs can be controlled to some extent by the feed ratio of monomer to the coinitiator. It is noteworthy that polydispersity index (PDI) of the free polymer in the presence of CNF-OH (5.86–1.99) is much broader than that in the control experiment without CNFs (1.19), and decreases with increasing the feed ratio. Similar phenomenon was also observed in the cases of CNTs.[24] By comparison, for the cases of functionalized CNTs by ATRP, PDI (1.77–3.57) increased with increasing the feed ratio, most likely due to more polymer coupling.[46]

For the cases without butyl alcohol, the grafted PCl content ($f_{wt\ \%}$) increased from 39.8 to 64.2 wt % when the mass feed ratio of monomer to CNF-OH was increased from 33.7/1 to 134.8/1 (Fig. 2 and Table I). Although no sacrificial initiator was added to the reaction system, free polymer ungrafted on CNFs was also obtained owing to the existence of tiny amount of water or glycol in the whole reaction system (including some adsorbed by the CNF-OH). From the weight of the free PCL, we calculated the mass fraction of sacrificial initiators (such as H_2O, etc.) in the whole reaction system is about 0.9–1 wt % of CNF-OH (Table I). The M_n of the free PCL was 5200 g/mol for CNF-PCL5 and 8270 g/mol for CNF-CPL6. Both values are not very high, mainly because the conversion of monomer is very low (10% for CNF-PCL5 and 5% for CNF-CPL6). Again, the M_n increased and PDI decreased with increasing the feed ratio. The comparative experiments showed that higher grafting efficiency can be achieved by using sole macroinitiator of CNF-OH.

Also, to ensure the higher initiation efficiency of the hydroxyl grafted on the surface of CNFs, butanol-initiated polymerizations of ε-caprolactone in the presence of CNF-COOH or pristine CNFs with the same synthesis approach and feed ratios were tried. For the case of pristine CNFs, TGA measurements showed that the lost weight below 500°C was lower than 1.5 wt %. For the case of CNF-COOH, the lost weight below 500°C was 15.5 wt %, because the carboxyl groups on the CNFs can also initiate the ROP of ε-caprolactone. While for the case of CNF-OH, the grafted content of PCL can achieve as high as 29.5 wt % (see CNF-CPL3 in Table I).

FTIR and NMR spectra

The chemical structure of the resulting PCL-grafted CNFs was analyzed by FTIR and NMR. Figure 3 shows the FTIR spectra of samples. The pristine CNFs show a peak at 1634 cm^{-1} corresponding to the sp^2 C=C stretching vibration. A small peak at 1715 cm^{-1} associated with C=O stretching vibration was observed for the CNF-COOH and CNF-OH, indicating the existence of carboxyl and ester groups on

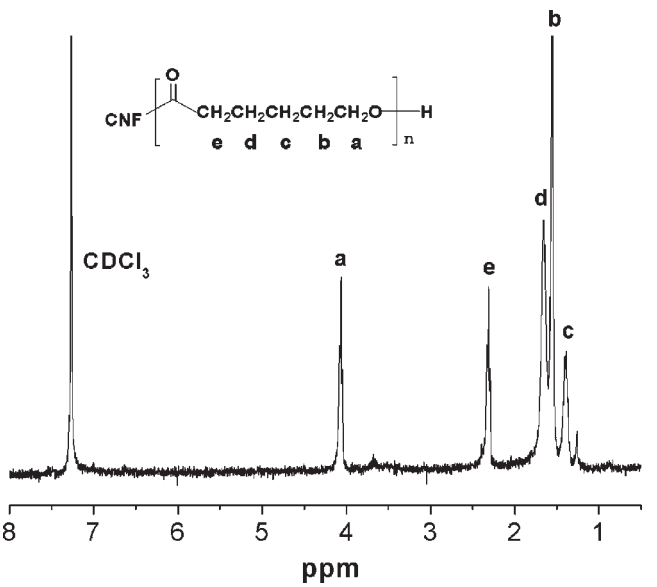

Figure 4 ^1H NMR spectrum of CNF-PCL4 (in $CDCl_3$).

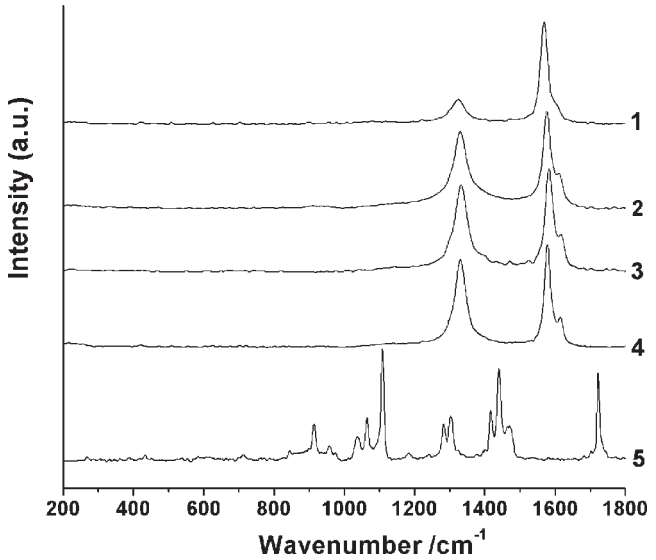

Figure 5 Raman spectra of (1) pristine CNFs, (2) CNF-PCL1, (3) CNF-PCL5, (4) CNF-PCL6, and (5) neat PCL.

CNF-COOH and CNF-OH, respectively. A strong carbonyl peak at 1725 cm^{-1} and two peaks at 2926 and 2866 cm^{-1} assigned to the sp^3 C—H stretching of PCL can be clearly observed for the PCL-grafted CNFs. These peaks are comparative with those of neat PCL.

Figure 4 displays the ^1H NMR spectra of the PCL-grafted CNFs. The proton peaks of the grafted PCL chains are found at δ 1.38 ppm (—$OCCH_2CH_2CH_2$ CH_2CH_2O—), 1.55 ppm (—$OCCH_2CH_2CH_2CH_2$ CH_2O—), 1.65 ppm (—$OCCH_2CH_2CH_2CH_2$ CH_2O—), 2.3 ppm (—$OCCH_2$—), and 4.1 ppm (—CH_2O—), respectively.

Raman spectra

It was shown that Raman spectrometer is also a powerful tool to characterize functionalized graphitic carbon materials.[24,47] Normally, a shoulder peak associated with covalently functionalized carbon materials can be observed beside G band (graphite mode).[24,27] In this article, Raman spectroscopy of the pristine and functionalized CNFs were also measured, as shown in Figure 5. The pristine CNFs display a weak D band (defect-induced mode) at 1328 cm^{-1} and a strong G band at 1569 cm^{-1}. The peak at 1328 cm^{-1} is probably due to the sp^3 hybridized carbon atoms located at open end and defects of CNFs.[37] The D to G band intensity ratio (I_D/I_G) for CNF-COOH (0.75) or CNF-OH (0.78) is much higher than that of pristine CNFs (0.23), implying the increase of defects after surface modification of CNFs. Similar to the phenomenon for the functionalized CNTs reported before,[24,27] a shoulder peak beside G band also appeared at $\sim$ 1615 cm^{-1} for the functionalized CNFs. Hence, this shoulder peak is assigned to D′ band. Clearly, the intensity of D′ band increases with increasing the content of PCL grafted on the surfaces of CNFs. In addition, the D, G, and D′ bands shift to higher wavenumber by about 3–10 cm^{-1} after functionalization. In Figure 5, strong Raman signals for the neat PCL are distinctly observed. However, such signals of neat PCL cannot be detected for the PCL-grafted CNFs. This is likely attributed because the covalently grafted PCL layer on the surface of CNFs is transparent and ultrathin.[27]

From the data and results of TGA, FTIR, NMR, and Raman spectra aforementioned, we can conclude that the surface-initiated ROP of ε-caprolactone has been successfully carried out, and PCL has been covalently grafted onto the surfaces of CNFs.

Dispersibility of PCL-grafted CNFs

The functionalized CNFs showed better dispersibility, wettability, or solubility than the pristine CNFs. The pristine CNFs are not wettable in polar solvent such as water (partially precipitate on the bottom and mostly float at the interface between water and air), while CNF-COOH and CNF-OH can be well wettable and partially dispersible in water because of the introduction of polar groups to the surfaces of CNFs, as shown in Figure 6(a). The dispersibility and solubility of PCL-grafted CNFs are greatly enhanced in solvent of low boiling point such as chloroform and THF. Figure 6(b) shows photographs of the same amount of CNFs and CNF-*g*-PCL (3 mg) dispersed in 10 mL of THF. The pristine CNFs can be slightly dispersed in THF after 5 min of sonication in a bath (40 Hz), but precipitated soon, and the two phases of CNFs and solvent can be observed clearly after a few hours. For the PCL-grafted CNFs, almost homogeneous phase was formed when the sample was dispersed in THF and can stay for several days. These tests also confirmed the covalent functionalization of CNFs.

SEM observation

The morphologies and structures of the functionalized CNFs were characterized by SEM. The representative

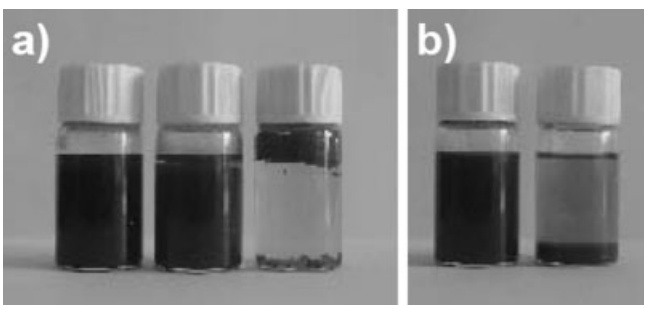

Figure 6 (a) Photographs of pristine CNFs (right), CNF-COOH (middle), and CNF-OH (left) placed in H_2O for 10 h. (b) Photographs of pristine CNFs (right) and CNF-PCL3 (left) placed in THF for 24 h.

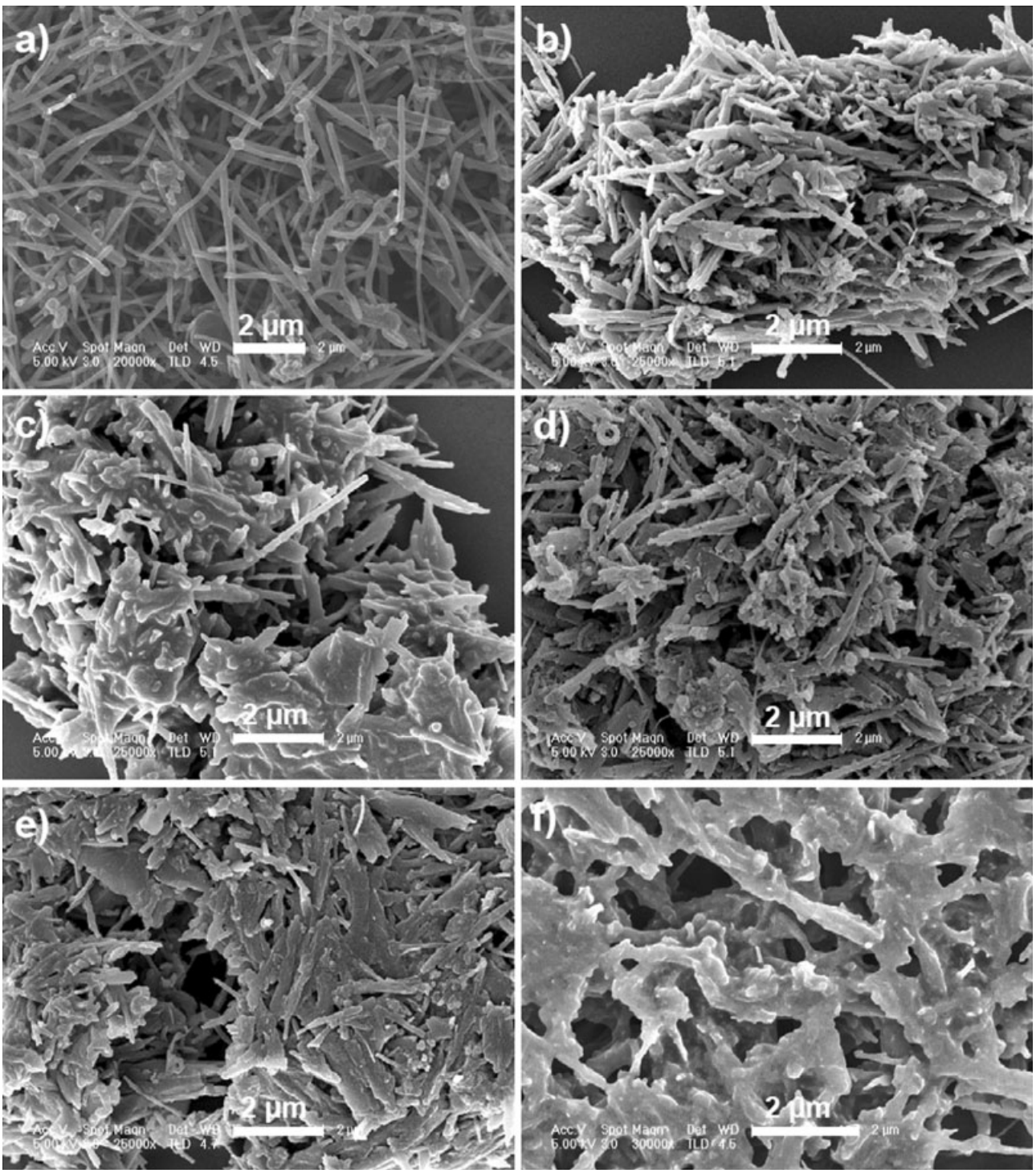

Figure 7 Representative SEM image of (a) pristine CNFs, (b) CNF-PCL1, (c) CNF-PCL2, (d) CNF-PCL3, (e) CNF-PCL5, and (f) CNF-PCL6.

SEM images are shown in Figure 7. For the pristine CNFs [Fig. 7(a)], individually separated straight and smooth rods, with a diameter of 100–200 nm, are observed. Almost every pristine CNF displays a protuberance at the end, which is resulted from the catalyst inducing growth of pristine CNFs. For the PCL-grafted CNFs [Fig. 7(b–f)], at least four distinct characters can be found when compared with the pristine CNFs: (1) the surface is much rougher, (2) the diameter is obviously bigger, or the rods become thicker, (3) individually separated rods are much less observed, and (4) the terminal protuberance cannot be observed any more. With increase of the grafted-polymer content, the rod-like CNFs become more illegible, because

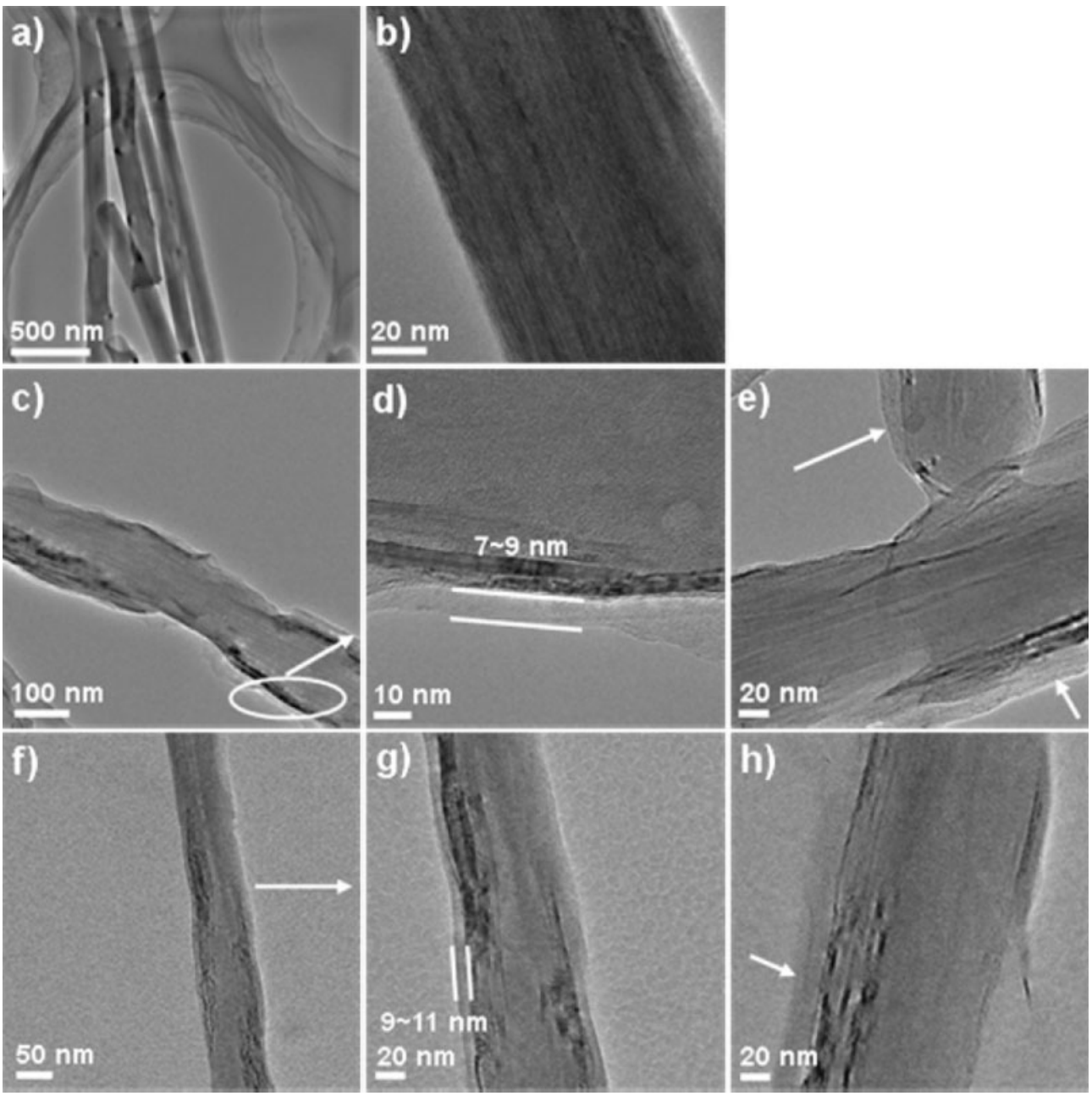

Figure 8 Representative TEM images of pristine CNFs (a,b), CNF-PCL4 (c–e), and CNF-PCL6 (f–h).

the polymer phase goes into more continuous and PCL makes more CNFs in clusters. This result is in accordance with that of the TGA data described earlier that the weight loss of PCL-grafted CNFs is from 19.8% to 64.2%. The SEM observations further proved the success of grafting PCL from surfaces of CNFs.

TEM observation

TEM, especially HRTEM, is a very useful tool to characterize core–shell structure and the thickness of polymer layer grafted on the surface of CNFs. Figure 8 shows the representative images of pristine CNFs and CNF-*g*-PCL. For the pristine CNFs, the surface is smooth, and only one phase of carbon is observed or no core–shell structure can be found [Fig. 8(a,b)]. For the PCL-grafted CNFs, two phases are observed with different image contrast [Fig. 8(c–h)]. The outer layer with lower gray is assigned to the polymer phase. From the different degree of gray, we can see clearly the core–shell structure for the polymer-coated CNFs. This indicates that the surface grafting of polymer is quite thorough. Similar core–shell structures were observed on the polymer-grafted CNTs prepared by the grafting from approach.[24,46] On the other hand, it is found that the thickness of the outer polymer layer

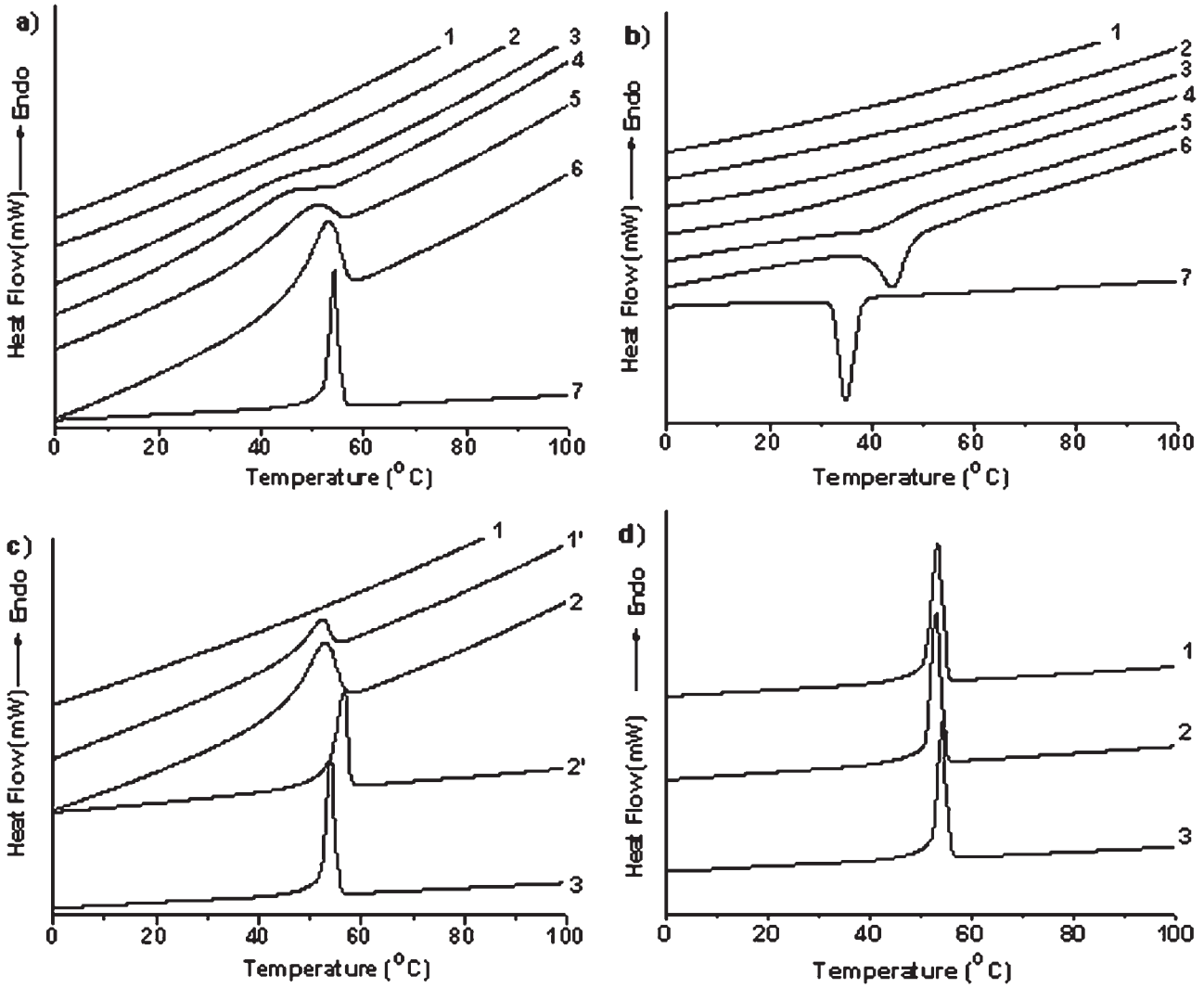

Figure 9 (a) DSC melting thermograms of (1) CNF-PCL1, (2) CNF-PCL2, (3) CNF-PCL3, (4) CNF-PCL4, (5) CNF-PCL5, (6) CNF-PCL6, and (7) neat PCL. (b) DSC crystallization thermograms of (1) CNF-PCL1, (2) CNF-PCL2, (3) CNF-PCL3, (4) CNF-PCL4, (5) CNF-PCL5, (6) CNF-PCL6, and (7) neat PCL. (c) DSC melting thermograms of (1) CNF-PCL1, (2) the mixture of 19.8 wt % PCL and CNF-OH (1′), CNF-CPL6, (3) the mixture of 64.2 wt % PCL and CNF-OH (2′), and neat PCL. (d) DSC melting thermograms of (1) free PCL1 (collected from the filtrate of CNF-PCL1), (2) free PCL2 (collected from the filtrate of CNF-PCL2), and (3) neat PCL.

is not the same as each other. As shown in Figure 8(d), the functionalized fiber of CNF-PCL4 has ~ 8 nm thickness of polymer layer; other two fibers of CNF-PCL4 display more than 15 nm thickness of polymer layer, as shown in Figure 8(e). The same instance is observed in the sample of CNF-PCL6. In Figure 8(f,g), the thickness of the polymer layer is ~ 9–11 nm; about 20 nm thickness of polymer layer is observed in Figure 8(h). The same phenomenon was found by other researchers for the graphitic CNFs functionalized by ATRP.[36] This could be caused by the following three factors: (1) the random or uneven distribution of initiating sites that are mainly localized at the defects of CNFs, (2) broad PDI of the grafted polymer, and (3) the different conformation and conglomeration of polymer chains on the nanosurfaces.

Crystallization and melting behaviors of the PCL-grafted CNFs measured by DSC

It is known that PCL is a crystalline polymer. Is it still crystalline and what are the crystallization features when PCL is tethered on a solid surface? To answer the questions and reveal more evidences for the covalent grafting, we measured the thermal properties of the PCL-grafted CNFs using DSC.

The melting temperature (T_m) of CNF-*g*-PCL and neat PCL can be obtained from DSC thermogram shown in Figure 9(a). The neat PCL (M_n = 4230 g/mol) displays a narrow endothermic melting peak at 55°C. Interestingly, for the samples of CNF-*g*-PCL, when the grafted polymer content is low, especially for CNF-PCL1 (19.8 wt %), CNF-PCL2 (21.9 wt %), no endothermic peak is observed. Similarly, when Scha-

dler and coworkers modified MWNTs with epoxide-based functional groups, no glass transition temperature (T_g) of MWNT-epoxide was observed.[48] With increase in the grafted PCL content, a broad endothermic melting peak appears; for the CNF-PCL6 (64.2 wt %), a clear melting peak is observed. With respect to the peak of the neat PCL, the melting peak of CNF-*g*-PCL is much broader.

The corresponding crystallization curves of the samples are shown in Figure 9(b). The crystallization temperature (T_c) of the neat PCL ($M_n = 4230$ g/mol) is about 35°C. For CNF-*g*-PCL, when the grafted polymer content is low (less than 32.7%), no crystallization peak is observed. With the rise of the PCL content, broad crystallization peak appears; when the PCL content reaches 64.2 wt %, distinct and broad crystallization peak at about 44°C is detected. The outcome from the crystallization measurements is in good agreement with that from the melting behaviors.

The disappearance or broadening of melting/crystallization peak can be possibly explained by the fact that when small amount of PCL is covalently attached to the CNFs, the movement of short PCL chains is greatly hindered, and ordered crystalline structure is difficultly formed. When the polymer content rises, it is easier to form ordered structure for longer polymer chains. Therefore, a melting peak of PCL can be observed. Because of the anchoring of polymer chains, their movement is still limited, leading to imperfect crystallization and broad melting peak as observed.

Two other possible factors associated with this phenomenon are also in our consideration: (1) the disappearance of the melting peak is due to the too small amount of PCL in CNF-*g*-PCL, (2) the broad melting peak for CNF-*g*-PCL with high PCL content is caused by broad PDI of PCL grafted on CNFs, since polydispersity of a polymer has influence on its crystallization behavior. To eliminate the first factor, 19.8 wt % of PCL (free polymer collected the preparation of CNF-PCL1) was blended with CNF-OH according to the TGA measurement data. From Figure 9(c), distinct melting peak at 53°C is observed, although it is relatively broad. When 64.2 wt % of PCL was mixed with CNF-OH, the endothermic peak becomes narrower, similar to the peak of the neat PCL. Obvious differences are found from the DSC measurements between the CNF-*g*-PCL and the mixtures. Therefore, the disappearance of the melting peak for the CNF-*g*-PCL is not mainly caused by the small amount of polymer but by the covalent anchoring. Moreover, we also measured the thermal property of the PCL with broad PDI to investigate the possible polydispersity effect. As shown in Figure 9(d), narrow melting peak is also observed for the free polymer of PCL1 (collected from the filtrate of CNF-PCL1, PDI = 5.86) or PCL2 (PDI = 4.71), and the melting curves are quite similar to that of the neat PCL (PDI = 1.19). Thus, we can conclude that the broadening effect aforementioned is not due to the broad PDI.

All of these results obtained from the DSC measurements further confirmed the covalent grafting between PCL and CNFs for the samples of CNF-*g*-PCL.

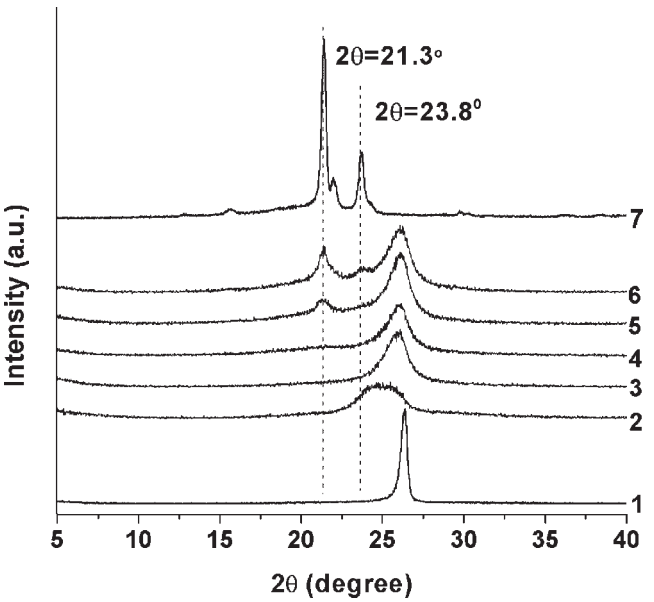

Figure 10 Wide-angle X-ray diffraction (WAXD) patterns of (1) pristine CNFs, (2) CNF-COOH, (3) CNF-OH, (4) CNF-PCL1, (5) CNF-CPL4, (6) CNF-PCL5, and (7) neat PCL.

Wide-angle X-ray diffraction

The crystallization properties of the neat PCL, the PCL-grafted CNFs, and the mixtures of CNF-OH and PCL were also examined by WAXD technique to confirm the DSC results. The XRD diagrams are shown in Figure 10. The neat PCL shows two intense reflection peaks at 2θ, 21.3° and 23.8°, associated with (110) and (200) facets, respectively, which is corresponding to orthorhombic crystalline form.[49] A characteristic crystallization peak of pristine CNFs at 2θ = 26.4° is observed due to the ''wall-to-wall'' *d* spacing of CNFs, which is indexed to (002) diffraction plane of hexagonal graphite.[37,50] After acid treatment of CNFs, the crystallization peak becomes broader, mainly because partial crystal structures of CNFs are broken and the degree of ordering becomes lower. Again, no PCL crystallization peak is observed for the CNF-*g*-PCL when the grafted polymer content is low (19.8 wt %, CNF-PCL1), and only a tiny peak of PCL at 2θ = 21.3° is found when PCL content reaches 32.7 wt %. With the increase of grafted polymer content, the peak at 2θ = 21.3° gets stronger and another crystallization peak at 23.8° can be observed. Both characteristic peaks of CNF-*g*-PCL are broader than those of the neat PCL,

because the presence of CNFs and lower degree of crystallization suffered from the fixing of one macromolecular chain end.

Comparatively, XRD diagrams of the mixtures of CNF-OH and PCL were also obtained (figure not shown). It is found that both peaks at 2θ (21.3° and 23.8°) can be clearly observed for the mixed sample with 19.8 wt % of PCL. For the sample mixed with 39.7 wt % of PCL, two narrow PCL crystallization peaks, similar to the peaks of the neat PCL, are shown. These results are in full agreement with those of DSC measurements described earlier. The comparative DSC and XRD results affirmatively proved that the absence or weakening/broadening of crystallization peak for the samples of CNF-*g*-PCL is not caused by the too low fraction of PCL but by the covalent grafting. This conclusion may be used to confirm the covalent linkage of crystalline polymer on nanosurfaces in reverse.

CONCLUSIONS

Functionalization of CNFs with biodegradable PCL by surface-initiated ROP of ε-caprolactone was successfully executed through importing hydroxy groups on surfaces of CNFs. This grafting-from strategy makes the content of grafted polymer controllable by adjusting the feed ratio of monomer to macroinitiator (CNF-OH). After surface functionalization, the D band of CNFs became stronger and a shoulder peak associated with the functionalization (D′) appeared at 1615 cm^{-1} in the Raman spectra. The intensity of such a shoulder peak increased with increase in the polymer content. The PCL Raman signals were not detected for the samples of PCL-grafted CNFs. SEM measurements showed that rod-like morphology became more indistinct when the grafted polymer content got higher, and continuous polymer phase embedded with CNFs was observed when the polymer content was high enough (>60 wt %). TEM measurements revealed the core–shell structure of CNF-*g*-PCL because of thorough polymer grafting. DSC and WAXD measurements gave more evidences for the covalent grafting from the obviously different results between CNF-*g*-PCL and the mixtures of CNFs and PCL. When the grafted polymer content is low, no or only small crystallization peak was observed in the DSC curves and XRD diagrams because of the fixing of one polymer end and low degree of crystallization. The resulting CNF-*g*-PCL can be well dispersed in the low-boiling-point organic solvents such as THF and chloroform. Because of the biodegradation and biocompatibility of PCL and graphitic carbon materials, the CNF-*g*-PCL hybrids promise a bright application in bionanotechnology and composites such as tissue engineering and three-dimensional cell culture. The relevant works are in progress and will be reported later.

We thank Dr. Yi Zheng Jin (Cambridge University) for helpful contributions.

References

1. Kroto, H. W.; Heath, J. R.; O'Brien, S. C.; Curl, R. F.; Smalley, R. E. Nature 1985, 318, 162.
2. Iijima, S. Nature 1991, 354, 56.
3. Iijima, S.; Ichihashi, T. Nature 1993, 363, 603.
4. Robertson, S. D. Nature 1969, 221, 1044.
5. Krishnan, A.; Dujardin, E.; Treacy, M. M. J.; Hugdahl, J.; Lynum, S.; Ebbesen, T. W. Nature 1997, 388, 451.
6. Iijima, S.; Yudasaka, M.; Yamada, R.; Bandow, S.; Suenaga, K.; Kokai, F.; Takahashi, K. Chem Phys Lett 1999, 309, 165.
7. Jin, Y. Z.; Gao, C.; Hsu, W. K.; Zhu, Y.; Huczko, A.; Bystrzejewski, M.; Roe, M.; Lee, C. Y.; Acquah, S.; Kroto, H.; Walton, D. R. M. Carbon 2005, 43, 1944.
8. Gilmour, I.; Russell, S. S.; Arden, J. W.; Lee, M. R.; Franchi, I. A.; Pillinger, C. T. Science 1992, 258, 1624.
9. De Jong, K. P.; Geus, J. W. Catal Rev Sci Eng 2000, 42, 481.
10. Tasis, D.; Tagmatarchis, N.; Bianco, A.; Prato, M. Chem Rev 2006, 106, 1105.
11. Tsubokawa, N. Polym J 2005, 37, 637.
12. Wang, C.; Guo, Z. X.; Fu, S.; Wu, W.; Zhu D. Prog Polym Sci 2004, 29, 1079.
13. Liu, T.; Jia, S.; Kowalewski, T.; Matyjaszewski, K.; Casado-Portilla, R.; Belmont, J. Langmuir 2003, 19, 6342.
14. Jin, Y. Z.; Gao, C.; Kroto, H. W.; Maekawa, T. Macromol Rapid Commun 2005, 26, 1133.
15. Sun, Y. P.; Zhou, B.; Lin, Y.; Wang, W.; Fernando, K. A. S.; Pathak, P.; Meziani, M. J.; Harruff, B. A.; Wang, X.; Wang, H.; Luo, P. G.; Yang, H.; Kose, M. E.; Chen, B.; Veca, L. M.; Xie, S. Y. J Am Chem Soc 2006, 128, 7756.
16. Djenizian, T.; Balaur, E.; Schmuki, P. Nanotechnology 2006, 17, 2004.
17. Qin, S.; Qin, D.; Ford, W. T.; Resasco, D. E.; Herrera, J. E. J Am Chem Soc 2004, 126, 170.
18. Kong, H.; Gao, C.; Yan, D. J Am Chem Soc 2004, 126, 412.
19. Gao, C.; Vo, C. D.; Jin, Y. Z.; Li, W. W.; Armes, S. P. Macromolecules 2005, 38, 8634.
20. Baskaran, D.; Mays, J. W.; Bratcher, M. S. Angew Chem Int Ed 2004, 43, 2138.
21. Kong, H.; Li, W. W.; Gao, C.; Yan, D.; Jin, Y.; Walton, D. R. M.; Kroto, H. W. Macromolecules 2004, 37, 6683.
22. Haggenmueller, R.; Fischer, J. E.; Winey, K. I. Macromolecules 2006, 39, 2964.
23. Xu, Y. Y.; Gao, C.; Kong, H.; Yan, D. Y.; Jin, Y. Z.; Watts, P. C. P. Macromolecules 2004, 37, 8846.
24. Zeng, H. L.; Gao, C.; Yan, D. Y. Adv Funct Mater 2006, 16, 812.
25. Qu, L. W.; Veca, L. M.; Lin, Y.; Kitaygorodskiy, A.; Chen, B. L.; McCall, A. M.; Connell, J. W.; Sun, Y. P. Macromolecules 2005, 38, 10328.
26. Park, C.; Ounaies, Z.; Watson, K. A.; Crooks, R. E.; Smith, J.; Lowther, S. E.; Connell, J. W.; Siochi, E. J.; Harrison, J. S.; St Clair, T. L. Chem Phys Lett 2002, 364, 303.
27. Gao, C.; Jin, Y. Z.; Kong, H.; Whitby, R. L. D.; Acquah, S. F. A.; Chen, G. Y.; Qian, H.; Hartschuh, A.; Silva, S. R. P.; Henley, S.; Fearon, P.; Kroto, H. W.; Walton, D. R. M. J Phys Chem B 2005, 109, 11925.
28. Xia, H.; Song, M. J Mater Chem 2006, 16, 1843.
29. Baibarac, M.; Baltog, I.; Godon, C.; Lefrant, S.; Chauvet, O. Carbon 2004, 42, 3143.
30. Koshio, A.; Yudasaka, M.; Zhang, M.; Iijima, S. Nano Lett 2001, 1, 361.
31. Cao, L.; Yang, W.; Yang, J.; Wang, C.; Fu, S. Chem Lett 2004, 33, 490.

32. Choi, Y. K.; Sugimoto, K. I.; Song, S. M.; Endo, M. Mater Lett 2005, 59, 3514.
33. Fan, Y.; Liao, B.; Liu, M.; Wei, Y.; Lu, M.; Cheng, H. Carbon 1999, 37, 1649.
34. Chai, G. S.; Yoon, S. B.; Yu, J. S. Carbon 2005, 43, 3028.
35. Vieira, R.; Pham-Huu, C.; Keller, N.; Ledoux, M. J. Chem Commun 2002, 954.
36. Li, L.; Lukehart, C. M. Chem Mater 2006, 18, 94.
37. Baek, J. B.; Lyons, C. B.; Tan, L. S. Macromolecules 2004, 37, 8278.
38. Baker, S. E.; Tse, K. Y.; Hindin, E.; Nichols, B. M.; Clare, T. L.; Hamers, R. J Chem Mater 2005, 17, 4971.
39. Jang, J.; Bae, J.; Choi, M.; Yoon, S. H. Carbon 2005, 43, 2730.
40. Li, J.; Vergne, M. J.; Mowles, E. D.; Zhong, W. H.; Hercules, D. M.; Lukehart, C. M. Carbon 2005, 43, 2883.
41. Gan, Z. H.; Liang, Q. Z.; Zhang, J; Jing, X. B. Polym Degrad Stab 1997, 56, 209.
42. Carrot, G.; Rutot-Houze, D.; Pottier, A.; Degee, P.; Hilborn, J.; Dubois, P. Macromolecules 2002, 35, 8400.
43. Flesch, C.; Delaite, C.; Dumas, P.; Bourgeat-Lami, E.; Duguet, E. J Polym Sci Part A: Polym Chem 2004, 42, 6011.
44. Dubois, P.; Krishnan, M.; Narayan, R. Polymer 1999, 40, 3091.
45. Lepoittevin, B.; Pantoustier, N.; Alexandre, M.; Calberg, C.; Jerome, R.; Dubois, P. J Mater Chem 2002, 12, 3528.
46. Kong, H.; Gao, C.; Yan, D. Macromolecules 2004, 37, 4022.
47. Jorio, A.; Pimenta, M. A.; Souza Filho, A. G.; Saito, R.; Dresselhaus, G.; Dresselhaus, M. S. New J Phys 2003, 5, 139.1.
48. Eitan, A.; Jiang, K.; Dukes, D.; Andrews, R.; Schadler, L. S. Chem Mater 2003, 15, 3198.
49. Wu, T. M.; Chen, E. C. J Polym Sci Part B: Polym Phys 2006, 44, 598.
50. Zou, G.; Zhang, D.; Dong, C.; Li, H.; Xiong, K.; Fei, L.; Qian, Y. Carbon 2006, 44, 828.